Eur Biophys J 21, 117–128 (1992)

European Biophysics Journal

The properties of ion channels formed by zervamicins

P. Balaram [1], K. Krishna [1], M. Sukumar [1], I. R. Mellor [2], and Mark S. P. Sansom [3]*

[1] Molecular Biophysics Unit, Indian Institute of Science, Bangalore 560 012, India
[2] Department of Life Science, University of Nottingham, University Park, Nottingham, NG7 2RD, UK
[3] Laboratory of Molecular Biophysics, The Rex Richards Building, University of Oxford, South Parks Road, Oxford, OX1 3QU, UK

Received December 12, 1991/Accepted March 13, 1992

Abstract. The zervamicins (Zrv) are a family of 16 residue peptaibol channel formers, related to the 20 residue peptaibol alamethicin (Alm), but containing a higher proportion of polar sidechains. Zrv-IIB forms multi-level channels in planar lipid (diphytanoyl phosphatidylcholine) bilayers in response to *cis* positive voltages. Analysis of the voltage and concentration dependence of macroscopic conductances induced by Zrv-IIB suggests that, on average, channels contain ca. 13 peptide monomers. Analysis of single channel conductance levels suggests a similar value. The pattern of successive conductance levels is consistent with a modified helix bundle model in which the higher order bundle are distorted within the plane of the bilayer towards a "torpedo" shaped cross-section. The kinetics of intra-burst switching between adjacent conductance levels are shown to be approximately an order of magnitude faster for Zrv-IIB than for Alm. The channel forming properties of the related naturally occurring peptaibols, Zrv-Leu and Zrv-IC, have also been demonstrated, as have those of the synthetic apolar analogue Zrv-Al-16. The experimental studies on channel formation are combined with the known crystallographic structures of Zrv-Al-16 and Zrv-Leu to develop a molecular model of Zrv-IIB channels.

Key words: Ion channel – Peptaibol – Channel forming peptide – Planar bilayer

Introduction

Over the past decade there has been a substantial increase in our understanding of the molecular properties of receptor-gated ion channels, concomitant with expansion of the sequence database for this superfamily of multi-subunit, trans-membrane proteins (Unwin 1989; Betz 1990; Stroud et al. 1990; Galzi et al. 1991). However, it has not yet proved possible to determine the high resolution structure of a representative of these proteins, despite the impressive progress in electron microscopic imaging of the nicotinic acetylcholine receptor (Toyoshima and Unwin 1988; Mitra et al. 1989). In lieu of a crystallographic structure of an intact channel protein, valuable insights into the molecular nature of the central pore region of channel proteins may be gained from studying simple model systems, namely channel-forming peptides (CFPs).

Channel-forming peptides are amphipathic peptides, of length ca. 20 residues, which adopt an α-helical conformation in the presence of lipid bilayers, and which form ion channels with electrophysiological properties comparable to those of channel proteins (Lear et al. 1988a; Oiki et al. 1990; Sansom 1991). A trans-membrane voltage induces CFPs to self-assemble within the plane of the bilayer to generate parallel bundles of transmembrane helices. The helices of a bundle surround a central pore, lining the latter with hydrophilic groups, and thus enabling permeation of selected ions. It is possible to relate functional (i.e. electrophysiological) properties of CFPs to structural (NMR and/or X-ray crystallographic) data in order to develop realistic models of channel structure (Sansom et al. 1991).

The peptaibols are a family of CFPs which contain a high percentage of the helix-promoting residue α-amino isobutyric acid (Aib). Each peptaibol molecule contains at least one proline residue, and the C-terminus is usually an α-amino alcohol e.g. phenylalaninol. Perhaps the most intensively studied peptaibol is alamethicin (Alm; Mathew and Balaram 1983; Hall et al. 1984; Boheim et al. 1987), a 20 residue CFP. However, Alm is rather hydrophobic, and so one might question the extent to which it mimics the amphipathic pore-lining helices of channel proteins. By contrast, the zervamicins (Zrv), a family of 16 residue peptaibols isolated from *Emericellopsis salmosynnemata* (Rinehart et al. 1981; Krishna et al. 1990), contain a higher proportion of hydrophilic sidechains, and thus might be considered closer models.

The sequences of three naturally occurring zervamicins (Zrv-IIB, -IC and -Leu) and of a synthetic analogue

Abbreviations: Alm, Alamethicin; Zrv, Zervamicin; CFP, Channel forming peptide; Aib, α-aminoisobutyric acid.

* *Correspondence to*: M. S. P Sansom

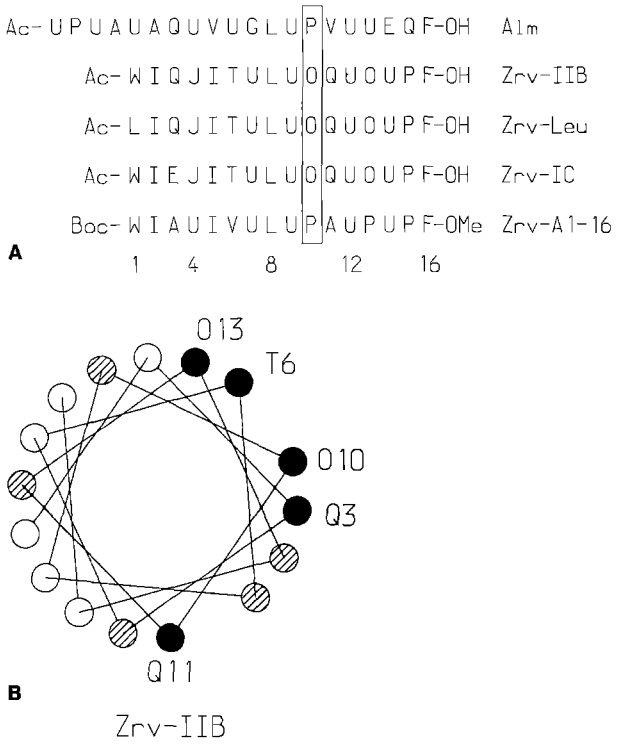

Fig. 1. **A** Comparison of the amino acid sequences of zervamicins and of alamethicin. The standard one-letter code is used, with the following additions: J = isovaline; O = hydroxyproline; and U = α-aminoisobuityric acid. The following abbreviations are used for terminal groups: Ac = acetyl; Boc = *t*-butoxycarbonyl; −OH = C-terminal amino alcohol; and −OMe = C-terminal methyl ester. The vertical box highlights the alignment of the central proline (or hydroxyproline) residue responsible for inducing a kink in the corresponding helices. **B** Helical wheel projection of the sequence of Zrv-IIB. Fully shaded circles represent hydrophilic residues, and hatched circles represent Aib residues

(Zrv-A1-16) are presented in Fig. 1 A, alongside the sequence of Alm. The natural Zrvs contain several hydroxyl group bearing residues. Some important residues are conserved between the two families of peptaibols, namely a C-terminal phenylalaninol, a polar residue at position 3 of Zrv (corresponding to Q7 of Alm) and a proline or hydroxyproline at position 10 of Zrv (P14 of Alm). Note that in Zrv-A1-16 all hydrophilic sidechains have been replaced by hydrophobic equivalents.

The crystal structures of Zrv-A1-16 (Karle et al. 1987), of Zrv-Leu (Karle et al. 1991) and of Alm (Fox and Richards 1982) have been determined at high resolution. All three structures are largely helical, with a central kink introduced into the molecule by the proline/hydroxyproline at position 10. The sequence of Zrv-IIB is shown on a helical wheel projection in Fig. 1 B. It can be seen that the helix is amphipathic, all of the polar residues lying on one face of the helix. This distribution of sidechains is typical of CFPs.

The crystal structures of the zervamicins have been compared in some detail, and a preliminary account of some of their channel forming properties presented in an earlier publication (Agarwalla et al. 1992). In this paper we provide a detailed description of the biophysics of zervamicin channels, and attempt to relate the channel properties to a preliminary molecular model of the structure of the helix bundle (Sansom et al. 1991, 1992).

Methods

1) Purification and synthesis of zervamicins

Zrv-IIB, -IC, and -Leu were purified from a crude isolate of *Emericellopsis salmosynnemata* using reverse phase HPLC as described by Krishna et al. (1990). Zrv-A1-16 was synthesised by conventional solution phase procedures, and purified by silica gel column chromatography (Sukumar 1987). Homogeneity of the peptides was established by the presence of a single peak upon analytical HPLC on a C_{18} column, and by one and two dimensional ^{1}H NMR at 270 MHz.

2) Bilayer measurements

Planar lipid bilayers were formed at the tip of glass microelectrodes using the method of Coronado and Latorre (1983), as described in Mellor and Sansom (1990). The lipid employed was diphytanoyl phosphatidylcholine (Avanti Polar Lipids, Birmingham, Alabama). The electrolyte solution used in all experiments was 0.5 M KCl, 10 mM BES (N,N-*bis*[2-hydroxyethyl]-2-aminoethanesulphonic acid), pH 7.0. The recording system was a List EPC7 patch-clamp amplifier, with output directed to a Sony PCM linked to a video recorder. All potentials refer to the *cis* compartment, i.e. the inside of the microelectrode, which contained the peptide solution. The *trans* compartment, i.e. the bath solution, was linked via a KCL/agar bridge to an Ag/AgCl electrode which was connected to ground.

Data analysis was performed on a Masscomp MC 5500 computer, using programs written in Fortran 77. Recordings were filtered at 1 to 3 kHz on playback, and sampled at 10 kHz prior to storage on disc. Analysis was as in previous publications (Mellor et al. 1988; Mellor and Sansom 1990).

3) Molecular modelling

Modelling was carried out using Quanta 3.0 (Polygen, Waltham, MA) run on a Silicon Graphics Personal Iris 4D25T workstation. All other programs were written in Fortran 77. Helix bundle generation and analysis of ion-channel interactions were carried out as described in Sansom et al. (1991).

Results

Zervamicin-IIB

1) Channel formation at positive potentials. Channel formation by Zrv-IIB was tested by exposing a bilayer to *cis* peptide and imposing a square wave potential of varying

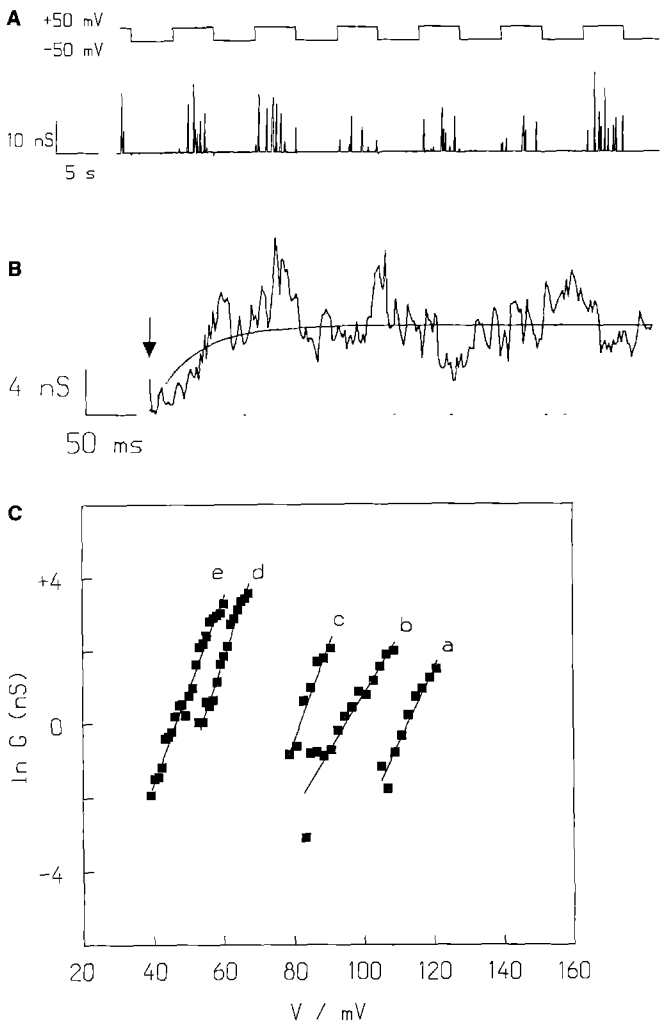

Fig. 2. **A** Zrv-IIB activated by *cis* positive potentials. A bilayer was exposed to *cis* 0.55 μM Zrv-IIB. A square wave potential (frequency 0.1 Hz, amplitude ±50 mV) was imposed (upper trace). Bursts of multilevel channel openings are seen at positive potentials, but not at negative potentials (lower trace). **B** Averaged Zrv-IIB (0.55 μM) current in response to +50 mV pulses (duration 0.5 s). The fitted single exponential (smooth curve) has a time constant of 41 ms. **C** Relationship between Zrv-IIB induced conductance (G) and membrane potential (V), established from steady-state current-voltage curves generated using triangular voltage waves (frequence 0.01 Hz). Five Zrv-IIB concentrations were employed: (a) 0.11; (b) 0.16; (c) 0.22; (d) 0.27; and (e) 0.33 μM. From analysis of this data (see text) the mean number of peptide monomers per channel was estimated to be $\langle N \rangle = 13.8$

amplitude and frequency. For example, in the experiment illustrated in Fig. 2A a peptide concentration of 0.55 μM was used, and a square potential wave of ±50 mV. The frequency of the wave was 0.1 Hz, providing +50 mV pulses of 5 s duration. It is evident that channel activity was only induced by *cis* positive potentials. All of the +50 mV pulses yielded multiple conductance level bursts of up to 10–15 nS in magnitude, whereas none of the −50 mV pulses induced channel activity. Increasing the amplitude of the pulses, e.g. to ±100 mV, still failed to elicit channel activity at *cis* negative potentials.

The effect of varying the pulse frequency was explored in order to obtain information on the rate of channel activation. If the frequency was increased to 1 Hz (0.5 s pulses), most, but not all, of the +50 mV pulses elicited one or more bursts of channel openings. Raising the frequency to 10 Hz (50 ms pulses) resulted in only a few positive pulses generating channel openings. Thus channel activation seemed to occur on a timescale of ca. 50 ms. This was explored in more detail by averaging currents elicited in response to 0.5 s pulses. The results of averaging are shown in Fig. 2B. It is evident that the conductance rises to a maximum within the first 50 ms and then fluctuates about an average value. The rising phase was fitted with a single exponential function, with a time constant of 41 ms. Averaging of currents elicited by a 0.1 Hz wave (not shown) revealed a similar rapid initial rise in conductance. There was no evidence for any further, slow increase in average current over the remainder of the 5 s pulse duration.

2) Macroscopic properties of Zrv-IIB induced conductance. Steady-state conductance-voltage relationships were obtained over a range of Zrv-IIB concentrations (0.11 to 0.33 μM) by imposing a triangular potential wave across the bilayer. The wave frequency was 0.01 Hz, and the amplitude (±V) was adjusted at each peptide concentration so as to yield maximal channel activation at the positive extreme whilst avoiding bilayer rupture. As in the voltage pulse experiments, channel activity was elicited by *cis* positive potentials, but not by *cis* negative potentials. As the peptide concentration was increased, the voltage required to activate Zrv-IIB channels decreased.

The theory of concentration and voltage dependence of peptaibol-induced conductance has been described in some detail by e.g. Hall et al. (1984). Only a brief account, sufficient for understanding of analysis of Zrv-IIB channel formation, is provided here. The dependence of macroscopic, steady-sate conductance (G) on voltage (V) and on peptide concentration (P) is given by:

$$G = \Gamma P^{\langle N \rangle} \exp\left(\frac{V}{V_e}\right),$$

where Γ is a constant dependent upon the peptide species, the bilayer composition and the electrolyte used, where $\langle N \rangle$ is the *average* number of helices/bundle, and where V_e is the change in potential required to generate an e-fold increase in conductance. Furthermore, $V_e = kT/e\langle N \rangle \alpha$, where α is the gating charge per peptide monomer. From analysis of the concentration dependence of conductance-voltage relationships, estimates of $\langle N \rangle$ and α may be obtained. V_e may be obtained from the reciprocal of the slope of a graph of $ln\,G$ against V. The concentration dependence of conductance is analyzed by defining a critical conductance, e.g. 1 nS, and for each concentration measuring the voltage required to induce this conductance, V_c. If one then defines V_a as the shift in V_c produced by an e-fold increase in peptide concentration, V_a may be obtained simply from a graph of V_c against $ln\,P$. Finally, $V_a = \langle N \rangle V_e$, and so estimates of $\langle N \rangle$ and α may be obtained.

The results of such an analysis of Zrv-IIB conductance-voltage relationships is shown in Fig. 2C. The average slope for the five lines yielded an estimate of

$V_e = 4.52$ mV, i.e. an increase in potential of 4.52 mV causes an e-fold increase in conductance. This is quite a marked voltage dependence. Analysis of the concentration dependence of V_c yielded an estimate of $V_a = 62.4$ mV. Together, these yielded parameter estimates of $\langle N \rangle = 13.8$ and $\alpha = 0.41$. Thus, *on average*, Zrv-IIB channels contained ca. 13 to 14 peptide monomers, and upon activation each monomer transferred an effective charge of +0.41 across the bilayer from the *cis* to the *trans* face.

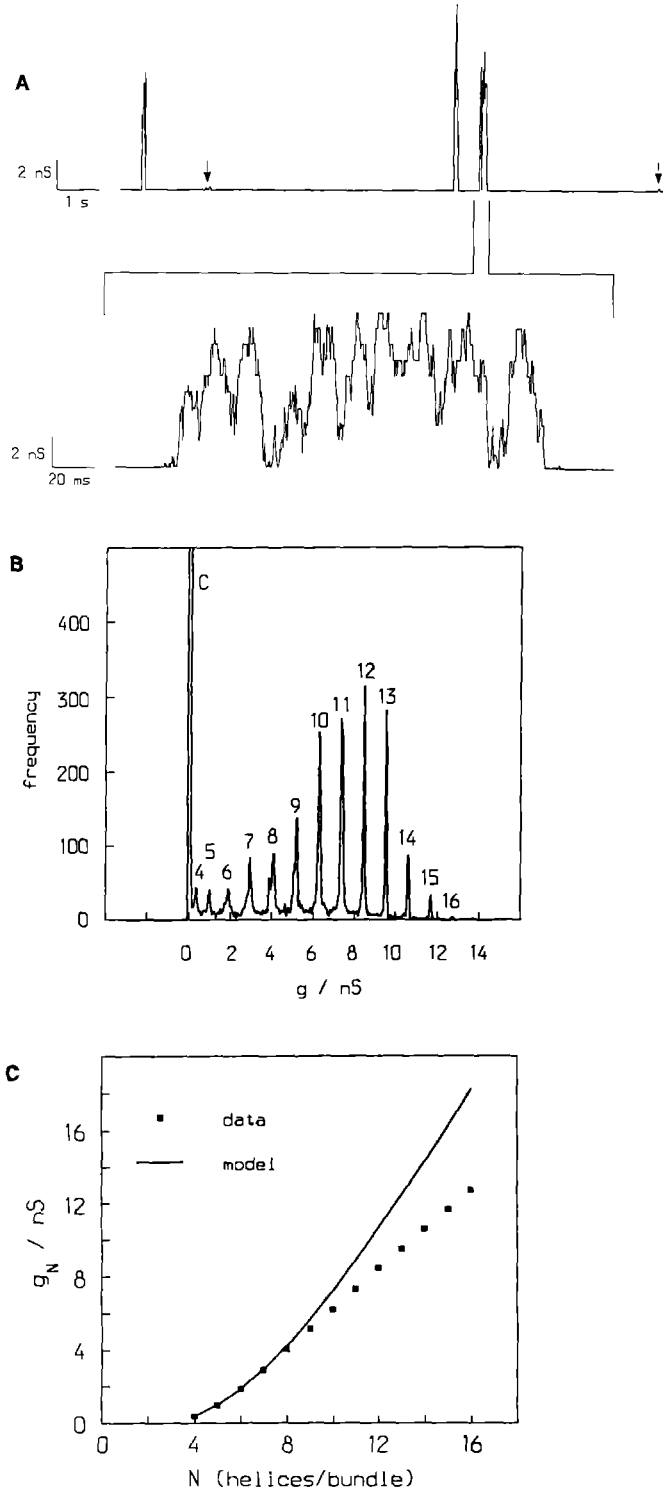

3) Single multilevel Zrv-IIB channels. The previous experiments provided information on the *macroscopic* properties of Zrv-IIB channels. By examining in detail single bursts of Zrv-IIB channel activity, it is possible to derive a *microscopic* model of Zrv-IIB channel formation.

Figure 3 A illustrates the results of an experiment in which a planar bilayer, formed at the tip of a microelectrode, was exposed to *cis* 1.1 μM Zrv-IIB, and held at a transbilayer potential of +175 mV. The long timebase trace shows three discrete, multilevel bursts of channel activity, separated by extended periods during which the channel is closed (i.e. zero conductance). There are also two bursts of channel activity which fail to reach higher conductance levels (indicated by arrows). The third multilevel bursts is shown on an expanded timebase. Multiple conductance levels within the bursts can clearly be seen. Detailed inspection reveals that transitions only occur between adjacent levels. This behaviour is comparable to that observed with alamethicin (Boheim 1974), and generates the stepwise progression of conductance levels within the burst.

Conductance levels were analyzed in more detail via evaluation of conductance histograms, as illustrated in Fig. 3 B. There are 13 different conductance levels, ranging from 350 pS equivalent to 3.8×10^8 ions s^{-1} at +175 mV) to ca. 12 nS (equivalent to 1.3×10^{10} s^{-1}). The lower conductance levels are comparable to what are generally thought of as channels, whereas the higher levels more closely resemble large electrolyte-filled pores. By comparison with the predictions of a simple equivalent-cylinder model (below), the lowest ($g = 350$ pS) conductance level may be equated with an $N = 4$ zervamicin helix bundle, in which case the highest level corresponds to an $N = 16$ bundle. On this basis, the modal conductance level corresponds to an $N = 12$ bundle. This is in good agreement with the estimate of $\langle N \rangle = 13.8$ obtained from the macroscopic analysis (above).

The progression of conductance levels observed in the histogram can be analyzed in terms of a simple equivalent-cylinder model for channel formation by helix bundles (Mellor and Sansom 1990; Sansom 1991). In this, the channel is approximated by a cylindrical pore of length l and radius a which runs down the centre of a bundle of

Fig. 3. **A** Discrete bursts of multilevel Zrv-IIB channels. A bilayer was exposed to *cis* 1.1 μM Zrv-IIB and the potential held at +175 mV. In the upper trace three multilevel bursts can be seen, plus two small groups of openings to the lower conductance levels only (indicated by arrows). The lower trace illustrates the third burst on an expanded timebase. Switching between multiple conductance levels is evident. **B** Conductance histogram derived from the recording illustrated in A. Numbers above the peaks correspond to N, the number of helices/bundle, assuming that the lowest conductance level ($g = 350$ pS) corresponds to an $N = 4$ bundle. **C** Conductance levels (g_N) as a function of helices/bundle (N). The points correspond to data taken from the histogram in B. The curve corresponds to an equivalent cylinder model (see text), with helix diameter = 1.0 nm, helix length = 2.4 nm, and electrolyte resistivity = 0.13 Ωm. Agreement between model and data is good for $N = 4$ to 8, but for higher levels the model predicts a greater conductance than is observed experimentally

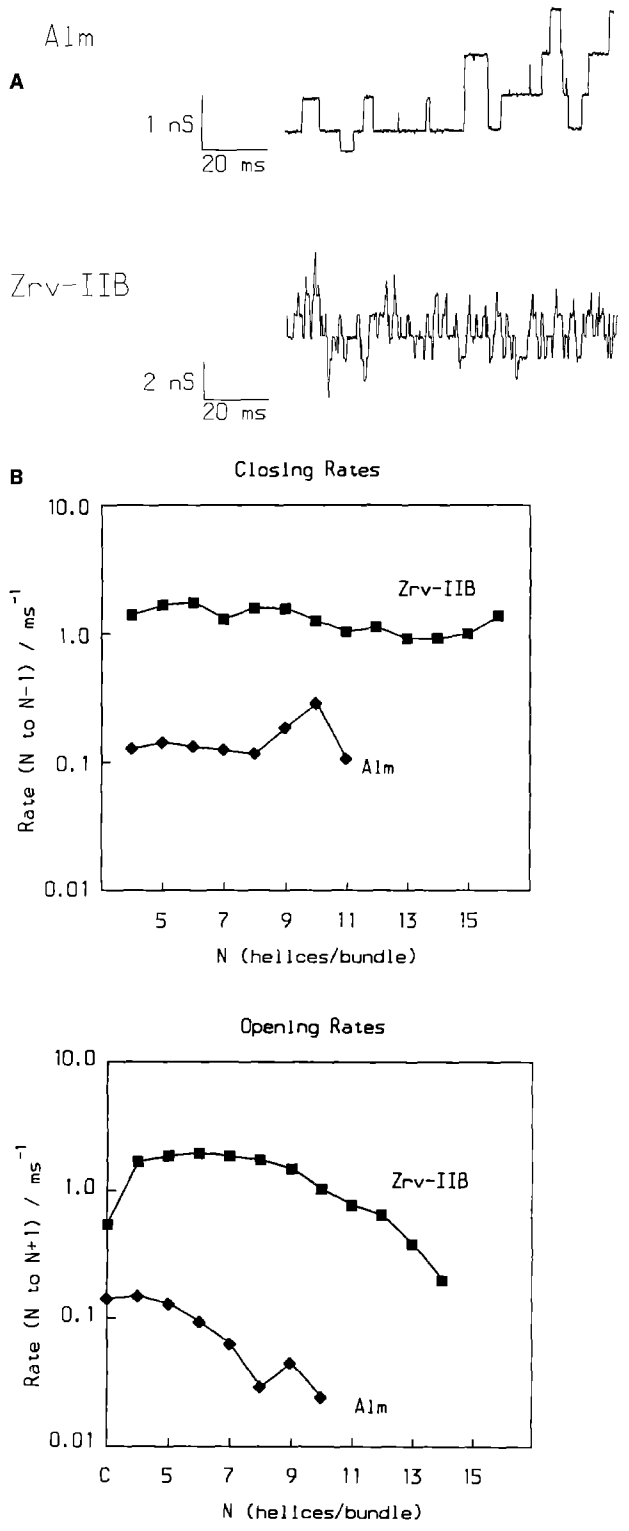

Fig. 4. **A** Comparison of the kinetics of Alm and Zrv-IIB channel activity. Both traces represent sections from discrete multilevel bursts of channel activity in the presence of 0.26 μM Alm at +125 mV, or of 1.1 μM Zrv-IIB at +175 mV. The overall level of channel activity in the two cases was approximately equivalent. It is evident that switching between adjacent levels occurs much more frequently with Zrv-IIB (see Table 1). **B** Results of statistical analysis of kinetic data. Both Alm and Zrv-IIB recordings were analyzed, using the methods described in the text, in terms of the gating model: $O_{N-1} \overset{k_{N,N-1}}{\longleftarrow} O_N \overset{k_{N,N+1}}{\longrightarrow} O_{N+1}$. It is evident that both closing rates ($k_{N,N-1}$) and opening rates ($k_{N,N+1}$) are approximately an order of magnitude higher for Zrv-IIB than for Alm

N helices, and is filled with electrolyte of resistivity ϱ. The conductance of such a pore (Hille 1984) is given by:

$$g = \frac{\pi a^2}{\varrho(l + \pi a/2)}.$$

The radius of the central pore is given by:

$$a = \frac{R}{\sin(\pi/N)} - R.$$

For a 16-residue α-helix, $R = 1.0$ nm and $l = 2.4$ nm. The resistivity of 0.5 M KCl is 0.13 Ωm (Robinson and Stokes 1965). The resultant sequence of conductance levels is shown in Fig. 3C, alongside the observed values for Zrv-IIB. For $N = 4$, the calculated value of $g = 380$ pS and the observed value of $g = 350$ pS are in good agreement. The model and data remain in agreement for $N = 4$ to 8. For $N > 8$, the predicted conductance is higher than the observed conductance, until for $N = 16$, the predicted $g = 18$ nS whereas the observed $g = 12$ nS. Thus the simple model appears to adequately account for the lower conductance levels, i.e. lower N bundles, but not for the higher levels. This is discussed in more detailed below.

4) Kinetics of Zrv-IIB channels. Macroscopic kinetics of Zrv-IIB channel activation in response to a voltage jump have already been discussed. This section is concerned with the microscopic kinetics of switching between adjacent conductance levels, i.e. the kinetics of the transitions $O_N \rightarrow O_{N+1}$ and $O_N \rightarrow O_{N-1}$, where O_N is an open channel bundle of N monomers. These transition rates correspond to an important component of the kinetics of assembly/disassembly of helix bundles, namely the kinetics of addition/removal of helices to/from a bundle.

The kinetics of switching of Alm and Zrv-IIB are compared visually in Fig. 4A. The two traces represent expanded sections from recordings which showed discrete bursts of channel openings, and which were approximately equivalent in terms of overall levels of activity. It is evident that switching between adjacent conductance levels occurs more frequently for Zrv-IIB than for Alm, i.e. transition rates are higher for the former.

Some measure of differences in kinetics may be obtained from the overall statistics summarised in Table 1. This presents kinetic data averaged across all conductance levels. A *burst* of channel openings was defined as being preceded and followed by closings of duration greater than a preset minimum for interburst intervals. The minimum interburst intervals used were 30 mS for Alm and 10 ms for Zrv-IIB. Here we are concerned principally with the kinetics of switching *within* bursts, i.e. intraburst kinetics. Within a burst, a sojourn is defined as the period during which a channel remains in a given conductance level without transitions to adjacent levels. From Table 1 it can be seen that the bursts are shorter for Zrv-IIB than for Alm, and that there are more sojourns/burst. Strikingly, the mean sojourn duration for Alm is about 10× that for Zrv-IIB.

The kinetics of Alm and of Zrv-IIB were analyzed in more detail using a modification of the maximum likelihood procedure of Ball and Sansom (1989), as outlined in

Table 1. Channel gating kinetics. A burst is defined by return of the channel to the closed state (i.e. zero current) for a period of longer than 30 ms (for Alm), or of 10 ms (for Zrv-IIB)

	Alm	Zrv-IIB
Total number of bursts	35	12
Total number of sojourns	3393	2783
Mean number of sojourns/burst	97	232
Mean burst duration (ms)	446	100
Mean sojourn duration (ms)	4.6	0.43
SD of sojourn duration (ms)	6.3	0.59

Appendix A, in order to yield estimates of transition rates, $k_{N,N\pm1}$, as functions of N. The results of such analysis are presented in Fig. 4B. The main conclusion to be drawn is that, for all values of N, transitions rates for Zrv-IIB are about one order of magnitude higher than those for Alm. Secondly, closing rates ($k_{N,N-1}$) are largely independent of N, whereas opening rates ($k_{N,N+1}$) tend to decrease as N increases, suggesting that it is more difficult for a helix to add to a large bundle than to a smaller one. Overall, analysis of Zrv-IIB channel kinetics provides detailed information on the assembly/disassembly process.

Related zervamicins

1) Zervamicin-Leu. Zrv-Leu is closely related to Zrv-IIB. The two peptides differ only in the substitution of a leucine for a tryptophan sidechain at residue 1. This is a conservative substitution in that one bulky hydrophobic sidechain is replaced by another.

The two peptides also closely resemble one another in their functional properties. Zrv-Leu channels are activated at *cis* positive potentials, and occur in discrete multilevel bursts. Two such bursts of channel openings are depicted in Fig. 5. On a 1 s timebase, it can be seen that the maximum conductance of the burst is ca. 4 nS. On an expanded timebase, discrete conductance levels may be resolved. However, transitions between adjacent levels occur more frequently than for Zrv-IIB, and consequently there are more brief, incompletely resolved sojourns. This prevented detailed kinetic analysis, and also resulted in rather broad peaks in the conductance histogram (not shown). Consequently, analysis of conductance levels was not as clear cut as for Zrv-IIB. In particular, it was not possible to unambiguously identify a low conductance level, corresponding to the ca. 350 pS openings of Zrv-IIB. Overall, seven conductance levels were resolved, ranging from 0.92 nS to ca. 4 nS. Conductance level increments ranged from 0.47 to 0.64 nS, somewhat smaller than the corresponding values for Zrv-IIB. Thus, although there Zrv-IIB and Zrv-Leu are qualitatively similar in their channel forming activity, there are some minor quantitative differences.

2) Zervamicin-IC. Zrv-IC differs more markedly from Zrv-IIB in that the glutamine sidechain at position 3 is replaced by a glutamate. Thus an negative charge is introduced into the otherwise neutral molecule, close to the N-terminus of the helix. This structural change is paralleled by a change in functional properties.

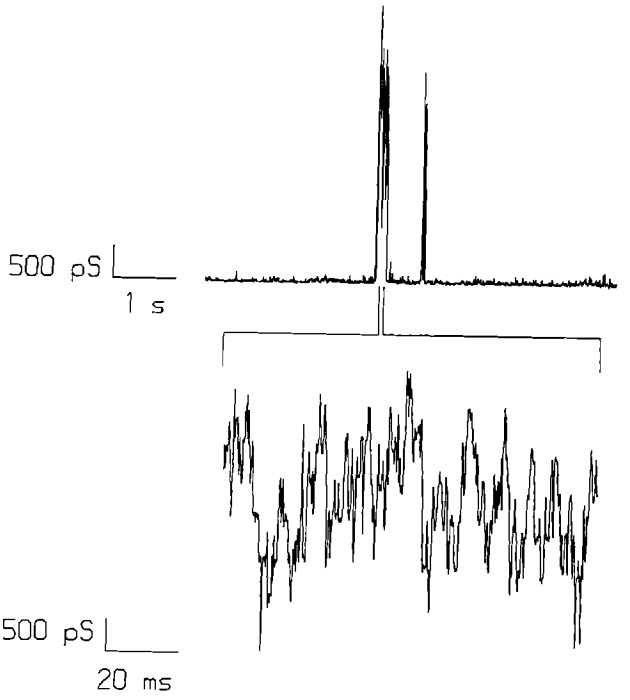

Fig. 5. Zrv-Leu channels. The peptide concentration was 0.57 μM, and the bilayer potential +100 mV. Discrete bursts of channel openings are seen, comparable to those observed with Zrv-IIB. On an expanded timebase rapid switching between adjacent conductance levels is observed

Zrv-IC channels are activated at *cris* negative potentials. Figure 6A depicts a recording made in the presence of 0.5 μM Zrv-IC at −50 mV. The channel activity is continuous, rather than discrete bursts of channel openings as observed with the previous two peptides. Up to 5 conductance levels are seen, although given the continuous activity it is not possible to exclude the possibility that such a recording represents simultaneous activity of more than one helix bundle. The maximum conductance level is ca. 1.9 nS, and the transitions between adjacent levels are ca. 0.4 nS. There are only brief, incompletely resolved sojourns in the first conductance level and in the closed state, and so detailed kinetic analysis was not possible.

A further experiment was carried out to confirm that Zrv-IC channels were activated at *cis* negative potentials. A voltage ramp from +140 to −140 mV was imposed upon a bilayer exposed to a low concentration (0.06 μM) of Zrv-IC (Fig. 6B). No channels were activated at positive potentials. At −75 mV, a burst of channel activity was initiated, and two further bursts followed at lower voltages. Unfortunately, it was not possible to obtain steady-state conductance-voltage relationships using this peptide, but the results confirm the *cis* negative activation suggested by the constant potential experiments.

3) Zervamicin-A1-16. Zrv-A1-16 is a synthetic apolar analogue of the naturally occuring zervamicins. All of the polar residues of Zrv-IIB are replaced by hydrophobic sidechains. In particular, the two glutamine sidechains at positions 3 and 11 are replaced by alanines. It was there-

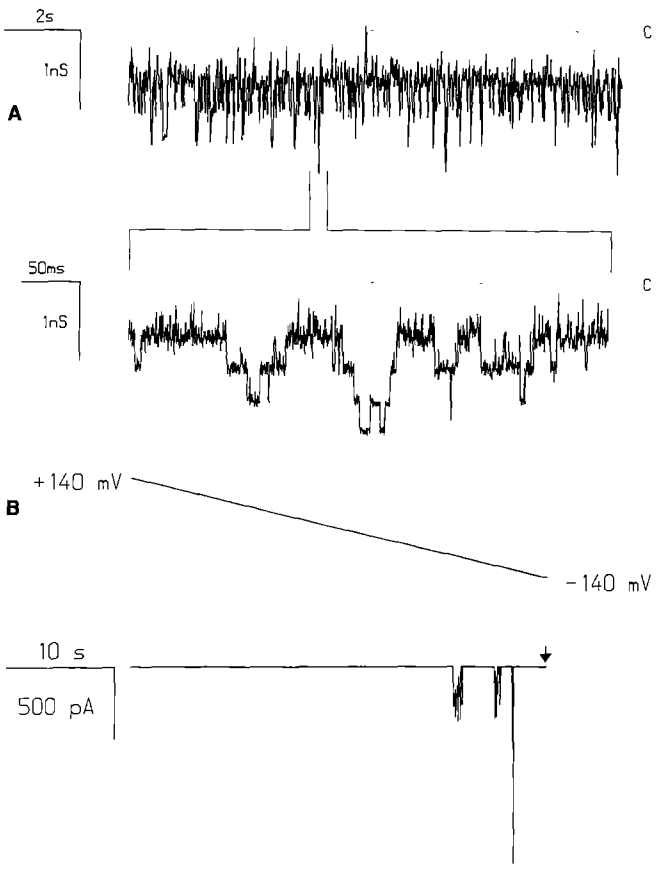

Fig. 6. **A** Zrv-IC channel openings. The peptide concentration was 0.5 μM, and the bilayer potential −50 mV. Continuous channel activity is seen rather than discrete bursts. Up to 5 conductance levels are evident. Transitions to the closed state (C, indicated by the dotted line) are brief and incompletely resolved. **B** Zrv-IC channel activity is induced at *cis* negative potentials. A bilayer exposed to 0.06 μM Zv-IC was subjected to a voltage ramp from +140 to −140 mV (upper trace). A burst of channel openings was initiated at −75 mV. The membrane broke at the potential indicated by the arrow

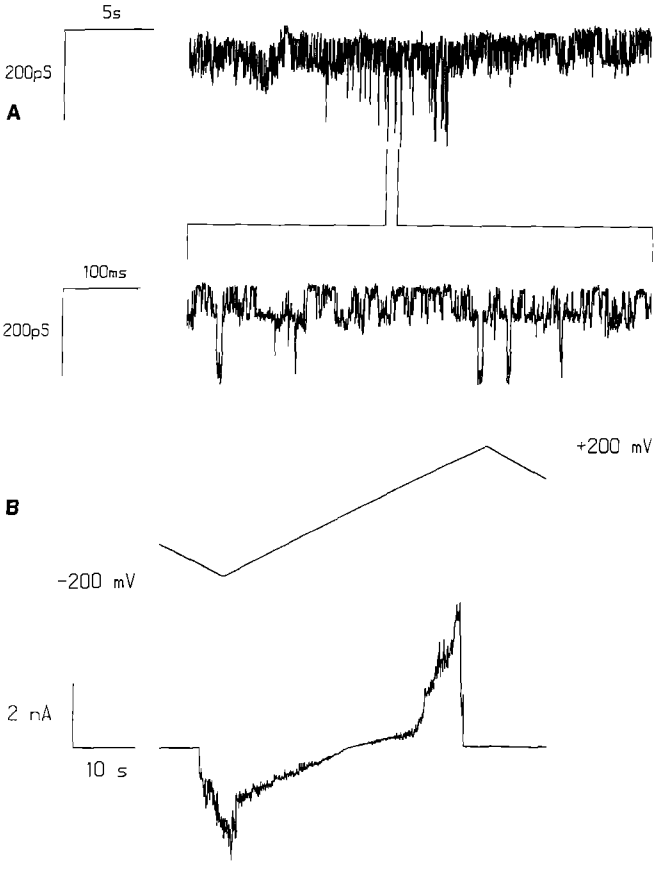

Fig. 7. **A** Zrv-A1-16 channels. Peptide was incorporated directly into the bilayer forming solution, at a peptide:lipid molar ratio of 1:100. The recording, made at −150 mV, illustrates continuous channel activity. On the expanded timebase, channel openings to two levels are evident. **B** A bilayer containing Zrv-A1-16 (P:L = 1:100) was subjected to a triangular voltage wave (frequency 0.02 Hz, amplitude ±200 mV, upper trace). Zrv-A1-16 channel activity can be seen at both positive and negative potentials, and seems to be at least partially voltage-dependent

fore of some interest to evaluate whether or not such a peptide would form ion channels.

The hydrophobicity of Zrv-A1-16 presented some problems with respect to bilayer experiments, as the peptide was insufficiently soluble in water to enable channel formation to be observed following exposure of the *cis* face of the bilayer to an aqueous solution of the peptide. Instead it proved necessary to incorporate the peptide directly into the bilayer. This was achieved by adding an aliquot of Zrv-A1-16 in ethanol to the solution of lipid in pentane used to form the bilayer. The nominal peptide:lipid molar ratio (P:L) was 1:100. In this manner it was possible to obtain Zrv-A1-16 channels, as illustrated in Fig. 7 A. The bilayer potential was −150 mV, although one would expect that the sign of the potential would not matter as direct incorporation would result in a symmetrical distribution of peptide between the two faces of the bilayer. Continuous channel activity may be seen, rather than discrete bursts. Inspection on an expanded timebase reveals two conductance levels. It is possible that there was a further level, intermediate between the two shown. The conductances were 63 and 192 pS, i.e. somewhat less than those observed with the other zervamicins. Detailed examination suggests that, as with the other peptides, transitions are only seen between adjacent levels i.e. there do not appear to be any direct openings of the channel to the higher conductance level. It would therefore seem that the apolar zervamicin is capable of forming channels, but that the characteristic stepwise progression through several conductance levels is not observed.

Figure 7 B shows the results of an experiment to investigate possible voltage activation of Zrv-A1-16 channels, using a ±200 mV triangular voltage wave. Channel activity appears to have both voltage dependent and voltage independent components. Furthermore, channel activity was not seen for every repeat of the voltage wave. The interpretation of this result is complicated by the direct incorporation of the peptide into the bilayer (see below).

Discussion

1) Voltage activation

Superficially, voltage activation of Zrv-IIB resembles that of Alm (Vodyanoy et al. 1983; Hall et al. 1984; Vodyanoy et al. 1988) in that both peptides are induced to form channels by *cis* positive potentials. In the case of Alm this behaviour is best explained in terms of re-orientation of the helix dipole (Hole et al. 1978; Schwarz and Savko 1982) in the imposed electric field (Boheim et al. 1983; Mathew and Balaram 1983; Sansom 1991). The negatively charged residue near the C-terminus (E18) is believed to anchor the C-terminus at the bilayer-water interface, and thus only when a *cis* positive potential is applied is the helix able to reorient itself in the bilayer, by repulsion of the formal positive charge (+1/2) at the N-terminus. In the case of Zrv-IIB the molecular interpretation underlying the experimental observations is less clear. Zrv-IIB contains no charged sidechains. So, it would seem that *cis* positive activation must result from some other means of anchoring the C-terminus of the molecule at the bilayer-water interface. One possibility is that the C-terminal hydroxyl group hydrogen-bonds to phosphate headgroups of lipid molecules. This might be tested by exploring analogues of Zrv-IIB with differing C-terminal groups. Molle et al. (1991) have recently explored analogues of Alm with varying substitutions at the C-terminus. They found no differences between the analogues in terms of rates of switching between conductance levels, but unfortunately did not comment on whether or not there were changes in the degree of channel activation by *cis* and by *trans* positive potentials.

The situation becomes more complex when one considers *cis* negative activation of Zrv-IC. Zrv-IC contains a negatively charged sidechain near the N-terminus (E3). There are two possible explanations for its voltage-dependent behaviour. The first is that, as with Zrv-IIB, the C-terminus remains anchored at the interface and *cis* negative potentials repel the charge on E3. This would result in the helix dipole being oriented unfavourably with respect to the electric field. The second possibility is that residue E3 anchors the N-terminus at the interface, and that the C-terminus (charge −1/2) is repelled by *cis* negative potentials, thus resulting in a favourable orientation of the dipole. At present it is difficult to distinguish between these two possibilities. An experimental test might be to replace E3 with a positively charged sidechain, e.g. lysine, and to determine whether the resultant peptide was activated by *cis* positive or by *cis* negative potentials.

The synthetic apolar peptide, Zrv-A1-16, provides valuable information concerning the mechanism of voltage activation of peptaibol channels. From data such as that in Fig. 7B it is evident that Zrv-A1-16 channel activity is voltage induced, despite the absence of any charged or polar sidechains. This confirms the important role of the helix dipole in peptaibol channel activation, and is in accord with the earlier work of Menestrina et al. (1986), who demonstrated channel formation by simple hydrophobic peptides constructed from repeats of the sequence motif A-U-A-U-A. It should be noted that in the case of Zrv-A1-16, voltage activation is observed even though the peptide is incorporated directly into the lipid solution from which the bilayer is formed. However, it is possible that once the bilayer is formed some of the peptide partitions out into the aqueous phase. Thus, although this experiment would seem to favour channel activation via helix reorientation, rather than via the mechanism proposed by Schwarz and coworkers (Rizzo et al. 1987; Stankowski et al. 1988) in which channel activation occurs via voltage-induced changes in partitioning of peptide between aqueous and bilayer phases, it is not conclusive. Further support for the helix reorientation model comes from oriented circular dichroism studies by Huang and Wu (1991).

2) Conductance levels

Conductance levels within Zrv-IIB channel bursts have been analyzed in some detail. The results are in agreement with the helix bundle ("barrel-stave") model, which proposes that successive conductance levels correspond to increases in N, the number of helices/bundle (Boheim 1974; Boheim et al. 1983; Mathew and Balaram 1983). When the model is expressed in terms of an equivalent cylinder conductance model (Sansom 1991), the agreement with the data is quite good for $N=4$ to 8. This in itself is gratifying, given the simplicity of the model. It suggests that the properties of Zrv-IIB channels are not too far removed from those of electrolyte-filled pores of equivalent dimensions. For values of N in excess of 8, the model predicts higher conductances than those which are observed. This is unlikely to result from approximating the channel as electrolyte filled pore, as this would be lead to larger errors for the *lower* conductance levels. This suggests that the assumption of an axially symmetrical bundle of helices breaks down for higher N values. We would suggest that for $N=4$ to 8, the centres of the helices lie on a regular N-gon, i.e. the pore is approximately circular in cross-section. At higher N values it is suggested that the bundle collapses to some extent, such that the central pore is distorted towards a "torpedo" (or extremely ellipsoidal) shape in cross-section. This would result in a lesser dependence of conductance on N for higher N values. The N value at which the transition between a circular and a torpedo-shaped pore occurs would be determined by the energetics of helix packing and of dipole-dipole repulsions of parallel helices.

It is of interest that the mean number of helices/bundle, $\langle N \rangle = 13.8$, is quite high for Zrv-IIB. This may be due to the mismatch in length of the bilayer (thickness ca. 40 Å) and of the peptide (length ca. 24 Å). Hall et al. (1984), studying the behaviour of Alm in bilayers of different thickness, found that $\langle N \rangle$ increased from ca. 2 in 14:1 lipid to ca. 11 in 20:1 lipid, i.e. $\langle N \rangle$ increased as the bilayer increased in thickness relative to the peptide. In an earlier study (Mellor and Sansom 1990), it was demonstrated that a 14 residue peptide, mastoparan, forms ion channels in diphytanoyl phosphatidylcholine bilayers, suggesting that a considerable degree of peptide-bilayer mismatch may be tolerated. The thermodynamics

of such mismatches have been analyzed by e.g. Mouritsen and Bloom (1984). It also should be noted that large numbers of successive conductance levels may also be observed with Alm. For example, Taylor and de Levie (1991) have observed up to 18 levels for "reversed" alamethicin channels (obtained at reduced temperatures and *cis* negative potentials).

One should consider to what extent Zrv-IIB channels may be considered as models of physiological ion channel proteins. It is clear that the higher conductance levels correspond to pores which are much larger than, and correspondingly less selective than, those formed by channel proteins. However, for $N=4$, the conductance in 0.5 M KCl is ca. 350 pS. Roughly, this corresponds to a conductance of ca. 140 pS in a physiological saline solution (ca. 0.2 M KCl). Comparison with conductance of e.g. 130 pS for locust muscle glutamate-receptor channels (Sansom and Usherwood 1990) and of 20–40 pS for nAChR channels (Hille 1984), suggests that the $N=4$ bundle is a realistic model of the central pores of ion channel proteins.

3) Kinetics

A detailed picture of Zrv-IIB kinetics, both at the macroscopic and the microscopic levels, has emerged as a result of these investigations. Macroscopic, voltage-jump studies yield time constants of the order of 50 ms for activation of Zrv-IIB conductance. These are comparable to the "slow" component of Alm channel activation in response to voltage-jumps, as identified by Boheim and Kolb (1978), which has been identified with fluctuations in the number of channels, i.e. with inter-burst fluctuations. In this aspect of channel kinetics Alm and Zrv-IIB seem to be closely comparable.

Zrv-Leu exhibits the same general pattern of conductance levels as Zrv-IIB, but the conductance increment between successive levels is somewhat smaller for the former peptide. It is possible that replacement of W1 in Zrv-IIB by L1 in Zrv-Leu results in a change in helix packing such that Zrv-Leu helix bundles are "squashed" at lower N values than for Zrv-IIB. Lower conductance level increments (ca. 0.4 nS) are also seen with Zrv-IC. There are two possible explanations for this. Firstly, interactions between the negatively charged E3 sidechain and permeant ions might be expected to result in a reduced conductance relative to that expected for an equivalent electrolyte filled pore. However, there is an experimental complication in that Zrv-IC channel activity occurs continuously, rather than in discrete bursts. Consequently, it is not possible to ascertain whether openings to multiple levels represent genuine multilevel openings of a single bundle, or whether they result from summation of independent, single-level openings.

Zrv-A1-16 is notable in that it does not seem to generate channel openings to more than two (or possibly three) conductance levels. This supports a role for polar, hydrogen-bonding residues in the stabilization of higher order peptaibol helix bundles, as suggested for Alm by Mathew and Balaram et al. (1983), and by Fox and Richards (1982).

In terms of its microscopic, intra-burst kinetics Zrv-IIB appears to be about an order of magnitude faster than Alm. There are two possible explanations of this. It may result from the greater degree of bilayer/peptide mismatch occurring with Zrv-IIB, which presumably requires some degree of local compression of the bilayer in order to accommodate the helix bundle. Alternatively, the proline and hydroxyproline residues present in the C-terminal half of Zrv-IIB, which are absent from the C-terminal sequence of Alm, may confer additional flexibility upon Zrv-IIB which in turn may support higher assembly/disassembly transition rates. In this context, it is interesting to note that substitution of Leu for Aib in a synthetic Alm analogue (Molle et al. 1988; 1991) also results in an approximately 10 fold increase in transition rates. Molecular dynamics investigations of the conformational flexibility of different peptaibols might be an approach to this question (see e.g. Fraternali 1990). Such studies might also help to rationalize the observation that W1 to L1 substitution in going from Zrv-IIB to Zrv-Leu leads to a further increase in rates of intra-burst transitions.

4) Molecular modelling

Some progress towards understanding channel formation by zervamicins and related peptaibols can be made via molecular modelling studies. This work is described in detail elsewhere (Sansom et al. 1991; 1992), and so the account here will only refer to those aspects of the model directly pertinent to an understanding of the experimental data. Modelling studies have been greatly aided by high resolution crystal sructures for two of the peptides – Zrv-A1-16 (Karle et al. 1987) and Zrv-Leu (Karle et al. 1991). The backbone conformations of these two peptides are very similar. The discussion here will focus on attempts to model Zrv-IIB pores, although Zrv-A1-16 will also be briefly discussed.

A model for the Zrv-IIB monomer has been developed based upon computer "mutation" of L1 in the crystal structure of Zrv-Leu to W1 in the Zrv-IIB model, followed by energy minimization of the W1 sidechain conformation. The resultant structure is shown in Fig. 8A. The concave face of the helix is hydrophobic, containing the sidechains of W1 and F16, whereas the convex face is hydrophilic, containing Q3 and Q11. A model for an $N=6$ Zrv-IIB bundle is shown in Fig. 8B. In arriving at this model, several factors have been taken into consideration. The helices are approximately parallel, as one would expect them to be when aligned by an electric field across the bilayer. In this particular model, the helices have been packed with their C-terminal segments parallel, thus generating the wider mouth of the channel at the N-termini of the monomers. Alternative packing arrangements have also be considered (Sansom et al. 1991; 1992). The helices are oriented such that the hydrophilic face is directed towards the centre of the pore, providing possible interaction sites for both water molecules and for permeant ions. Empirical calculations of interaction energies between the channel and a K^+ ion placed at different positions within the pore (Sansom et al. 1991; 1992; Sansom 1992 b) suggest possible (transient) binding

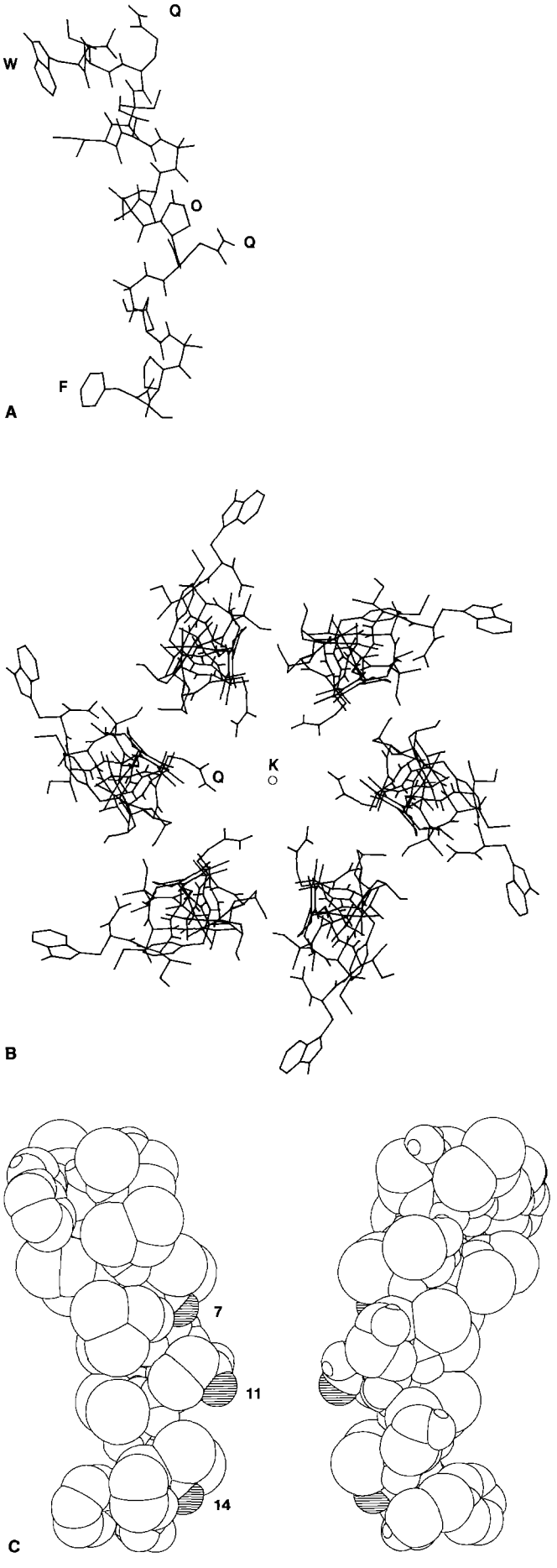

sites for the ion. Two solvent-exposed mainchain carbonyl oxygen atoms (O:7 and O:14) and the amide group of the sidechain of Q11 are capable of interacting favourably with a permeant cation. It appears that conformational flexibility of the sidechain of Q11 may play an important role in optimising such interactions (see also Agarwalla et al. 1992).

A similar class of models may be constructed for Zrv-A1-16 channels (Sansom et al. 1991). These go some way to explaining how this peptide, devoid of hydrophilic sidechains, forms ion permeable channels. In particular, it seems likely that the exposed mainchain oxygens, O:7 and O:14, provide ion-channel interaction sites. Such interactions may be of general relevance in the context of the presence of proline residues in membrane-spanning regions of a range of channel and transport proteins (Brandl and Deber 1986; Woolfson and Williams 1990; Woolfson et al. 1991; von Heijne 1991; Williams and Deber 1991; Sansom 1992a).

Overall, it is evident the zervamicins are well-suited to a detailed study of the relationship between channel structure and function. Crystal structures of several members of the family have been determined, and channel properties have been characterised. Preliminary modelling studies have proved promising. Future studies will focus on more detailed molecular modelling of channel structures and channel-ion interactions, and on design, synthesis and evaluation of "mutant" zervamicins.

Acknowledgements. This work was supported by the UK SERC and the Wellcome Trust (MSPS), and by the Department of Science and Technology, India (PB). We wish to thank Dr. I. L. Karle for providing the coordinates of Zrv-Leu in advance of their publication.

Appendix A – maximum likelihood analysis of gating kinetics

Gating of multilevel helix bundle channels may be modelled as:

$$\underset{0}{C} \rightleftharpoons \underset{1}{O_4} \rightleftharpoons \underset{2}{O_5} \rightleftharpoons \cdots \rightleftharpoons \underset{L}{O_{\max}},$$

where C is the closed channel (level 0), and where the open states of the channel (O_N, where N is the number of monomers in the helix bundle) range from level 1 ($N=4$) to level L ($N=\max$). Single channel data for a single *burst*

Fig. 8. **A** Zrv-IIB monomer, modelled on the basis of the crystal structure of Zrv-Leu (see text for details). The two aromatic sidechains (W1, and F16) can be seen to be on the concave face of the kinked helix, and the two glutamine sidechains (Q3 and Q11) on the convex face. The position of the kink-inducing hydroxyproline (O10) is also indicated. **B** $N=6$ bundle model of a Zrv-IIB channel, constructed as discussed in the text, and viewed down the z (i.e. pore) axis. The position of the sidechain of Q11 is labelled, as is that of a K^+ ion placed on the pore axis at $z=0$. **C** Two opposite monomers from the $N=6$ Zrv-IIB channel model, viewed down the y axis. Atoms are represented by their van der Waals radii, with non-polar carbons shown as extended atoms. The following oxygen atoms are shaded: O: 7, Oε1: 11 and O: 14

of openings starts and ends with level 0, and consists of $j=1$ to M sojourns, where the jth sojourn is in level s_j and is of duration t_j. Transitions are only allowed between adjacent levels, so that s_j is proceeded (followed) by $s_{j-1}=s_j\pm1$ ($s_{j+1}=s_j\pm1$). Note that this implies that $s_1=s_M=1$.

The probability density function for the sequence of M sojourns in a burst is given by:

$$f=\prod_{j=1}^{M}\left\{\exp\left[\frac{-t_j}{\tau_{s_j}}\right]\cdot k_{s_j,s_{j+1}}\right\},$$

where

$$\tau_{s_j}=(k_{s_j,s_j-1}+k_{s_j,s_j+1})^{-1} \quad \text{for} \quad 1\le s_j<L$$
$$=(k_{L,L-1})^{-1} \quad \text{for} \quad s_j=L$$

defines the mean sojourn time in level i. The likelihood is defined by $L=\ln(f)$, and so is given by:

$$L=-\sum_{j=1}^{M}\left[\frac{t_j}{\tau_{s_j}}\right]+\sum_{j=1}^{M}\ln(k_{s_j,s_{j+1}}),$$

where one should note that the summation is over the *sojourns*. This expression can be converted to a more useful form by changing to summation over the *levels*, giving:

$$L=-\sum_{i=1}^{L}T_i(k_{i,i-1}+k_{i,i+1})+\sum_{i=1}^{L}(F_{i,i-1}\ln k_{i,i-1}+F_{i,i+1}\ln k_{i,i+1}),$$

where T_i is the total time spent by the channel in level i, and where $F_{i,i\pm1}$ is total number of transitions from level i to level $i\pm1$. The maximum likelihood estimators of the rate constant, $\hat{k}$, are given by solving the equations

$$\frac{\partial L}{\partial k_{i,i\pm1}}=0 \quad \text{for} \quad i=1 \quad \text{to} \quad L,$$

which yields

$$\hat{k}_{i,i\pm1}=\frac{F_{i,i\pm1}}{T_i}.$$

The Hessian matrix (**H**) is defined by diagonal term of the form

$$\frac{\partial^2 L}{\partial k_{i,i\pm1}^2}=\frac{-F_{i,i\pm1}}{(k_{i,i\pm1})^2},$$

the off-diagonal terms being zero. This is inverted to yield the covariance matrix, $\mathbf{Cov}=(-\mathbf{H})^{-1}$, giving the variances of the rate constant estimates:

$$\mathrm{Var}(k_{i,i\pm1})=\frac{(\hat{k}_{i,i\pm1})^2}{F_{i,i\pm1}}.$$

References

Agarwalla S, Mellor IR, Sansom MSP, Karle IL, Flippen-Anderson JL, Uma K, Krishna K, Sukumar M, Balaram P (1992) Zervamicins, a structurally characterised peptide model for membrane ion channels. Biochem Biophys Res Comm (submitted for publication)

Ball FG, Sansom MSP (1989) Single channel gating mechanisms: model identification and parameter estimation. Proc R Soc Lond B 236:385–416

Betz H (1990) Homology and analogy in transmembrane channel design: lessons from synaptic membrane proteins. Biochemistry 29:3591–3599

Boheim G (1974) Statistical analysis of alamethicin channels in black lipid membranes. J Membr Biol 19:277–303

Boheim G, Kolb HA (1978) Analysis of the multi-pore system of alamethicin in a lipid membrane: I – Voltage-jump current relaxation measurements. J Membr Biol 38:99–150

Boheim G, Hanke W, Jung G (1983) Alamethicin pore formation: voltage-dependent flip-flop of α-helix dipoles. Biophys Struct Mech 9:181–191

Boheim G, Gelfert S, Jung G, Menestrina G (1987) α-Helical ion channels reconstituted into planar bilayers. In: Yagi K, Pullman B (eds) Ion transport through membranes. Academic Press, Tokyo, pp 131–145

Brandl CJ, Deber CM (1986) Hypothesis about the function of membrane-buried proline residues in transport proteins. Proc Natl Acad Sci USA 83:917–921

Coronado R, Latorre R (1983) Phospholipid bilayers made from monolayers on patch-clamp pipettes. Biophys J 43:231–236

Fox OR, Richards FM (1982) A voltage-gated ion channel model inferred from the crystal structure of alamethicin at 1.5 Å resolution. Nature 300:325–330

Fraternali F (1990) Restrained and unrestrained molecular dynamics simulations in the NVT ensemble of alamethicin. Biopolymers 30:1083–1099

Galzi JL, Revah F, Bessis A, Changeux JP (1991) Functional architecture of the nicotinic acethylholine receptor: from electric organ to brain. Ann Rev Pharmacol Toxicol 31.37–72

Hall JE, Vodyanoy I, Balasubramanian TM, Marshall GR (1984) Alamethicin: a rich model for channel behaviour. Biophys J 45:233–247

Hille B (1984) Ionic channels of excitable membranes, Sinauer, Sunderland, Mass

Hol WG, von Duijen PT, Berendsen HJC (1978) The α-helix dipole and the properties of proteins. Nature 273:443–446

Huang HW, Wu Y (1991) Lipid-alamethicin interactions influence alamethicin orientation. Biophys J 60:1079–1087

Karle IL, Flippen-Andersen J, Sukumar M, Balaram P (1987) Conformation of a 16-residue zervamicin IIA analog peptide containing 3 different structural features: 3_{10}-helix, α-helix and β-bend ribbon. Proc Natl Acad Sci USA 84:5087–5091

Karle IL, Flippen-Andersen J, Agarwalla S, Balaram P (1991) Crystal structure of Leu-zervamicin, a membrane ion channel peptide. Implications for gating mechanisms. Proc Natl Acad Sci USA 88:5307–5311

Krishna K, Sukumar M, Balaram P (1990) Structural chemistry and membrane modifying activity of the fungal polypeptides zervamicins, antiamoebins and efrapeptins. Pure Appl Chem 62:1417–1420

Lear JD, Wasserman ZR, DeGrado WF (1988) Synthetic amphiphilic peptide models for protein ion channels. Science 240:1177–1181

Mathew MK, Balaram P (1983) A helix dipole model for alamethicin and related transmembrane channels. FEBS Lett 157:1–5

Mellor IR, Thomas DH, Sansom MSP (1988) Properties of ion channels formed by *Staphylococcus aureus* δ-toxin. Biochim Biophys Acta 942:280–294

Mellor IR, Sansom MSP (1990) Ion channel properties of mastoparan, a 14 residue peptide from wasp venom, and of MP3, a 12 residue analogue. Proc R Soc Lond B 239:383–400

Menestrina G, Voges KP, Jung G, Boheim G (1986) Voltage-dependent channel formation by rods of helical peptides. J Membr Biol 93:111–132

Mitra AK, McCarthy MP, Stroud RM (1989) Three-dimensional structure of the nicotinic acetylcholine receptor and location of the major associated 43-kD cytoskeletal protein, determined at

22 Å by low dose electron microscopy and X-ray diffraction to 12.5 Å. J Cell Biol 109:755–774
Molle G, Dugast JY, Duclohier H, Spach G (1988) Conductance properties of des-Aib-Leu-des-Pheol-Phe-alamethicin in planar lipid bilayers. Biochim Biophys Acta 938:310–314
Molle G, Duclohier H, Julien S, Spach G (1991) Synthetic analogues of alamethicin: effect of C-terminal residue substitutions and chain length on the ion channel lifetime. Biochim Biophys Acta 1064:365–369
Mouritsen OG, Bloom M (1984) Mattress model of lipid-protein interactions in membranes. Biophys J 46:141–153
Oiki S, Madison V, Montal M (1990) Bundles of amphipathic transmembrane α-helices as a structural motif for ion-conducting channel proteins: studies on sodium channels and acetylcholine receptors. Proteins: Structure Funct Genet 8:226–236
Rinehart KL, Gaudioso LA, Moore ML, Pandey RC, Cok JC, Brber M, Sedgwick D, Bordoli RS, Tyler AN, Green BN (1981) Structures of eleven zervamicin and two emerimicin peptide antibiotics studied by fast atom bombardment mass spectroscopy. J Am Chem Soc 103:6517–6520
Rizzo V, Stankowski S, Schwarz G (1987) Alamethicin incorporation in lipid bilayers: a thermodynamic analysis. Biochemistry 26:2751–2759
Robinson AA, Stokes RH (1965) Electrolyte solutions. Butterworth, London
Sansom MSP, Usherwood PNR (1990) Single channel studies of glutamate receptors. Int Rev Neurobiol 32:51–106
Sansom MSP (1991) The biophysics of peptide models of ion channels. Prog Biophys Mol Biol 55:139–236
Sansom MSP (1992a) Proline residues in transmembrane helices of channel and transport proteins: a molecular modelling study. Prot Engineering 5:53–60
Sansom MSP (1992b) Sidechain-ion interactions in ion channels: a molecular modelling study. Biochem Soc Transac 20:2545
Sansom MSP, Kerr ID, Mellor IR (1991) Ion channels formed by amphipathic helical peptides – a molecular modelling study. Eur Biophys J 20:229–240
Sansom MSP, Balaram P, Karle IL et al (1992) Molecular modelling of ion channels formed by zervamicin-IIB (in preparation)
Schwarz G, Savko P (1982) Structural and dipolar properties of the voltage-dependent pore former alamethicin in octanol/dioxane. Biophys J 39:211–219
Stankowski S, Schwarz UD, Schwarz G (1988) Voltage-dependent pore activity of the peptide alamethicin correlated with incorporation in the membrane: salt and cholesterol effects. Biochim Biophys Acta 941:11–18
Stroud RM, McCarthy MP, Shuster M (1990) Nicotinic acetylcholine receptor superfamiliy of ligand-gated ion channels. Biochemistry 29:11009–11023
Sukumar M (1987) PhD Thesis, Indian Institute of Science, Bangalore
Taylor RJ, de Levie R (1991) "Reversed" alamethicin conductance in bilayers. Biophys J 59:873–879
Toyoshima C, Unwin N (1988) Ion channel of acetylcholine receptor reconstructed from images of post-synaptic membranes. Nature 336:247–250
Unwin N (1989) The structure of ion channels in membranes of excitable cells. Neuron 3:665–676
Vodyanoy I, Hall JE, Balasubramanian TM (1983) Alamethicin-induced current-voltage curve asymmetry in lipid bilayers. Biophys J 42:71–82
Vodyanoy I, Hall JE, Vodyanoy V (1988) Alamethicin adsorption to a planar lipid bilayer. Biophys J 53·649–658
von Heijne G (1991) Proline kinks in transmembrane α-helices. J Mol Biol 218:499–503
Williams KA, Deber CM (1991) Proline residues in transmembrane helices: structural or dynamic role? Biochemistry 30:8919–8923
Woolfson DN, Mortishire-Smith RJ, Williams DH (1991) Conserved positioning of proline residues in membrane-spanning helices of ion-channel proteins. Biochem Biophys Res Comm 175:733–737
Woolfson DN, Williams DH (1990) The influence of proline residues on α-helical structure. FEBS Lett 277:185–188